Electron spin resonance study of Si/SiGe quantum dots

F. Lipps, F. Pezzoli, M. Stoffel, C. Deneke, J. Thomas, A. Rastelli, V. Kataev, O. G. Schmidt, and B. Büchner
Leibniz Institute for Solid State and Materials Research, IFW Dresden, P.O. Box 270116, D-01171 Dresden, Germany
(Received 4 December 2009; revised manuscript received 5 February 2010; published 11 March 2010)

In this work, we present systematic electron spin resonance (ESR) experiments on SiGe quantum-dot structures. A series of samples with different sizes of quantum dots is prepared by varying growth temperature and spacing between quantum-dot layers. At a frequency of about 9.5 GHz, two ESR signals with g factors around 1.9992 and 1.9994 are observed with magnetic field in growth direction. The signals shift and broaden with magnetic field in the in-plane direction. The estimated dephasing time T_2^* amounts up to 500 ns. The saturation behavior yields relaxation time T_1 of about 10 μs. The relative intensity between the two peaks can be changed with illumination with subband-gap light. The two peaks are interpreted as s- and p-like states of electrons confined in the strained Si around the SiGe nanostructures.

DOI: 10.1103/PhysRevB.81.125312 PACS number(s): 76.30.−v, 73.21.La, 72.25.Rb, 72.20.Jv

I. INTRODUCTION

In contrast to III-V materials, the spin-orbit coupling in group IV semiconductors is fairly weak.[1] This enables long spin lifetimes and coherence times offering possibilities in spintronics applications and devices. Another limiting factor for relaxation and coherence times in III-V, namely, GaAs, semiconductor structures is the hyperfine interaction with the nuclear spins.[2] In Si and Ge, this effect is much smaller and can be further reduced by isotopic purification enabling even longer dephasing times.[3,4] Si and Ge are indirect semiconductors so optical methods are not best suited to study their electronic and spin states. Among other techniques, such as optical and electrical approaches, electron spin resonance (ESR) has emerged as a reliable and well-suited method to investigate spin states in semiconductors. ESR provides a direct access to static and dynamics of spin ensembles. In particular, information about the g factor and the dephasing and relaxation times can be extracted from continuous-wave ESR measurements.

ESR of bulk Ge and especially Si have been studied extensively in the past. Electrons contributing to an ESR signal can be localized on donors (e.g., phosphorus) embedded in Si or Ge.[3,5] In heavily n-doped bulk Si, the g factor is isotropic with $g=1.99875$ (Ref. 3) due to the singlet orbital ground state. In Ge, an isotropic g factor of $g=1.56$ is found.[6] However, if an uniaxial compressive strain is induced in the Si, higher states admix and the effective g factor is described by an axial symmetry tensor.[7]

Recent advances in strained layer epitaxial growth have allowed the fabrication of defect-free heterostructures, initiating novel investigations into low-dimensional physics. For instance, it has been shown that in SiGe-based heterostructures, a two-dimensional electron gas can be formed in strained Si channels.[8,9] ESR investigations pointed out that in these systems, the g factor and the linewidth is anisotropic as a result of the Bychkov-Rashba effect.[10]

More recently, it has been shown that for SiGe nanostructures coherently embedded in Si, the band-edge alignment is a type-II alignment.[11] This leads to localized confining potentials for electrons in the Si matrix.[12,13] As a consequence, self-assembled SiGe islands can assure a precise control and an external addressability to the localized electron spin states. In addition, the introduction of spin-resonance transistors based on SiGe nanostructures into the main stream Si technology opens up new degrees of freedom via band structure and strain engineering. Despite the large interest SiGe nanostructures have attracted, ESR investigations on such a system are still scarce. To our knowledge, there are only two experimental works reported in Refs. 14 and 15, whose results and their fundamental interpretation differ significantly. This makes a detailed and coherent study necessary to understand the behavior of the electronic states on SiGe nanostructures.

In this work, different SiGe quantum-dot (QD) structures were systematically studied with ESR. Two ESR peaks with different g-factor tensors were found around $g=1.999$. These spectral features are only observed in samples with quantum dots. Their spin dephasing time T_2^* is estimated to be on the order of 0.2–0.5 μs whereas the spin lifetime T_1 is on the order of 10 μs. The relative intensity of the ESR signals can be changed by illumination with infrared light, with energy below the gap of bulk Si and of the wetting layer. A qualitative model of the electronic structure of the heterostructures enables us to attribute the observed ESR signal to s and p states confined at the quantum dots.

Experimental details are given in Sec. II while the ESR results are presented in Sec. III. The electronic structure is modeled in Sec. IV and all results are discussed in Sec. V in summary.

II. EXPERIMENTAL

A. Sample structure

Two sets of SiGe/Si multilayers were grown by means of solid source molecular-beam epitaxy (MBE). After the deposition of a 100-nm-thick Si buffer on p-Si(001) substrates, fourfold stacks of 6.5 monolayers (MLs) and 8.5 ML of Ge separated by Si spacers were deposited at 600 °C and 700 °C, respectively. For each sample, the thickness of the Si spacers was constant and equal to 20, 70, or 100 nm. All the structures were capped with the same amount of Ge for further surface morphology investigations. It should be noted

 ©2010 The American Physical Society

that the samples are not intentionally doped, nevertheless we estimated a residual MBE background doping of about 2.3×10^{16} cm^{-3} (n type). As a consequence, to rule out spurious effects and to correctly assign the spectral features due to the presence of the dots, the following reference structures were grown in addition to the aforementioned samples: (i) a p-doped Si(001) substrate overgrown with 100 nm of Si buffer. (ii) Substrate and buffer with Ge wetting layers (WLs) grown at 600 °C, i.e., SiGe planar layers which form during the early stage of Ge deposition and always accompany the dots, separated by 20 nm of Si as in one of the multilayers. Since no dots are present, the Si can be considered as unstrained. (iii) A Si substrate overgrown with Si. The Ge layers were replaced by growth interruptions with duration equal to the time required to deposit Ge in the samples with dots.

The samples were characterized with atomic force microscopy (AFM) and transmission electron microscopy (TEM). Based on the gained structural information, single-band calculations were implemented to study the electronic structure of the heterostructures.

By varying the spacing between quantum-dot layers, the elastic coupling between layers changes.[16] For the samples with a 100 nm Si spacer grown at 700 °C, AFM characterization shows a monomodal distribution of islands indicating that no vertical alignment from one quantum-dot layer to the next occurs. Therefore the quantum dots and the confining potential in the Si induced by them can be regarded as isolated. The quantum dots are similar in shape and confining energy. This also holds for the sample grown at 600 °C with a spacing of 100 and 70 nm as corroborated by TEM analysis.

When decreasing the spacing between the dots, buried dots act—through the strain field—as favorable sites for the formation of dots in the higher layers. Because of that, there will be a change in intermixing and size between dots in different layers.[13,16] In general, intermixing and sizes are also larger for dots grown at higher temperatures. This explains why the dots grown at 600 °C and with 70 nm spacer still show a monomodal distribution.

In contrast, for the 70 nm sample grown at 700 °C, AFM images already show a widening of the size distribution of dots of the topmost layer. A vertical alignment takes place as confirmed by TEM [see Fig. 1(b)]. However a distance between the quantum dots in the vertical direction of more than 50 nm is still too large for an electronic coupling to occur.

B. ESR experiment

ESR spectra were measured in a standard X-band spectrometer from Bruker operating around a microwave frequency of 9.56 GHz. In addition to the applied external magnetic field, a small ac modulation field was applied. Samples were placed in a continuous-flow liquid-helium cryostat which enables measurements down to about 3.7 K. The cryostat was inserted in a rectangular TEM103 resonator with optical access for light illumination. The sample was located at the maximum of the magnetic field component of the microwave standing wave. The maximum sample size was

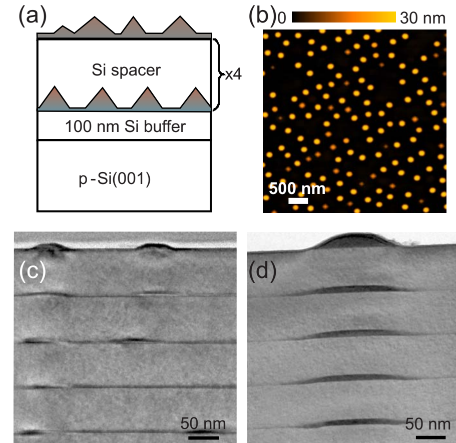

FIG. 1. (Color online) (a) Schematic sample structure; (b) AFM top view and (c) TEM of sample with 70 nm spacer grown at 600 °C. (d) Sample with 70 nm grown at 700 °C. Dots are much smaller in samples grown at lower temperatures.

8×4 mm^2 and up to four pieces of the same sample could be stacked. In order to ensure high-precision measurements, the spectrometer was equipped with an additional NMR sensor with accuracy of 10^{-3} Oe and an external frequency counter. Most of the measurements were performed at temperatures around 4 K due to high signal/noise ratio. Modulation amplitudes down to 0.01 Oe and modulation frequencies from 10 to 100 kHz were used in order to resolve the very narrow lines in the ESR spectra. Samples were illuminated with laser diodes at wavelengths of 1310 or 655 nm.

III. ELECTRON SPIN RESONANCE RESULTS

In an electron spin resonance experiment, the overall response of the sample is measured. Therefore great care has to be taken to separate an ESR signal attributed to SiGe nanostructures from signals originating from donors or impurities in the bulk substrate or in the deposited material, as well as effects caused by the boundaries between different materials.[17] The reference structures were measured to ensure that the observed signals are only due to the presence of the SiGe dots.

Surprisingly, in all our structures, the well-known signal of electrons on donors[6] in Si is not observed. This might be due to the fact that the absolute number of donors is on the order of the number of quantum dots but their ESR linewidth is about one order of magnitude broader than the ESR linewidth of quantum dots. This results in a weaker amplitude of the line. Furthermore, for the samples with quantum dots, the inhomogeneity of the sample may contribute to an additional broadening: Donors are distributed throughout the whole structure randomly. Thus, electrons on donors experience different strain. Since the repopulation effect between the donor states results in a reduction in hyperfine splitting with increasing strain,[7] their ESR signal is expected to broaden even more.

Figure 2 shows ESR spectra of a WL and a quantum-dot sample in the region around a g factor value of 2. The spectrum of the WL sample is representative for all reference

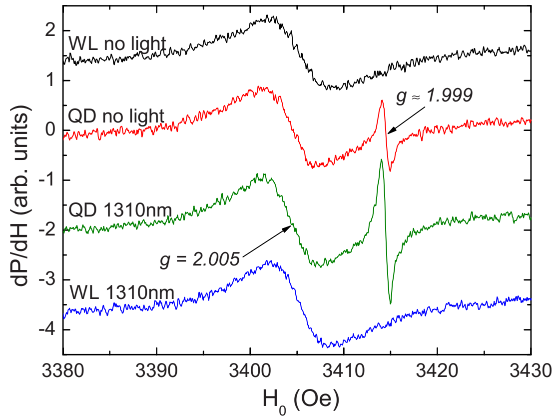

FIG. 2. (Color online) ESR spectra of a sample with only wetting layers and a sample with quantum dots; a narrow ESR peak is observed in the quantum-dot samples (QD) which is amplified under subband-gap light $\lambda=1310$ nm illumination; reference structures—here a sample with only wetting layers (WLs)—do not show the signal.

structures which show only a single peak with a linewidth $\Delta H_{pp}\approx 5$ Oe centered at $g\approx 2.005$. This signal is attributed to the oxidized sample surface since it is in good agreement with previous reports on ESR of dangling bonds of Si at the Si/SiO_2 interface.[18] In all quantum-dot samples, we observe an additional narrow peak, showing quantitative differences for the individual multilayer samples. This feature is absent in all reference structures. Therefore those signals are analyzed in more detail for the different quantum-dot structures.

A. Samples grown at 600 °C

All samples grown at 600 °C—with a silicon spacer thickness of 10, 20, 70, and 100 nm—give an ESR signal showing only a single Lorentzian line (*R*). For an incident microwave power P_{mw} of 1 mW, the line for the 100 nm sample (Fig. 3) shows a small anisotropy in *g* factor of

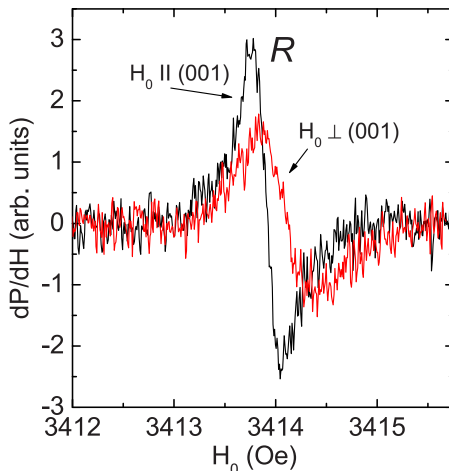

FIG. 3. (Color online) ESR signal (single peak) associated with dots in the sample grown at 600 °C with a spacer of 100 nm. The two spectra were taken with magnetic field oriented parallel and perpendicular to the growth direction (001).

TABLE I. *g* factors measured at $P_{mw}=1$ mW; the reproducibility is 3×10^{-5} for $g_\parallel$ and 4×10^{-5} for $g_\perp$; values marked with * are extrapolated from the fit around $g_\parallel$ shown in Fig. 5. For this, an axial symmetry of the *g* factor is assumed.

Sample	$g_\parallel$	$g_\perp$	Δg	g_0
600 °C, *R*				
20 nm	1.99925(2)	1.99912(2)	0.00013	1.99916
70 nm	1.99919(2)	1.99906(2)	0.00013	1.99910
100 nm	1.99917(2)	1.99906(2)	0.00011	1.99910
700 °C, *R*				
20 nm	1.99925(2)	1.99912*	0.00013	1.99916
70 nm	1.99926(2)	1.99914(2)	0.00012	1.99918
100 nm	1.99923(2)	1.99907(2)	0.00016	1.99912
700 °C, *L*				
20 nm	1.99941(2)	1.99923*	0.00018	1.99929
70 nm	1.99945(2)	1.99909*	0.00036	1.99921
100 nm	1.99943(2)	1.99892*	0.00051	1.99909

$\Delta g=g_\parallel-g_\perp=1.1(2)\times10^{-4}$ with the *g* factor being axially symmetric and an anisotropy in the linewidth ranging from $\Delta H_{pp\parallel}\approx 0.25$ Oe to $\Delta H_{pp\perp}\approx 0.45$ Oe. At higher powers, the line broadens and the signal starts to saturate.

The *g* anisotropy for all samples grown at 600 °C is the same within the experimental error [see later Fig. 5(a)] ranging from $\Delta g=1.1(2)\times10^{-4}$ to $1.3(2)\times10^{-4}$. However, the absolute values of the *g* factors are slightly higher for the 20 nm sample than for 70 and 100 nm spacing. *g* factors are listed in Table I. Control measurements carried out at another time show slightly different values of the *g* factor. This reproducibility is within an error of about $\delta g_\parallel=3\times10^{-5}$ and $\delta g_\perp=4\times10^{-5}$ but does not affect the anisotropy Δg.

B. Samples grown at 700 °C

All samples grown at 700 °C show a remarkable difference with respect to samples grown at 600 °C, i.e., two ESR peaks [see Fig. 4(a)]. This double-peak spectrum is a feature which has not been reported before.[14,15] The peaks are sharper than the single peak observed in samples grown at 600 °C. The relative intensity between the two peaks is the same for samples with 100 and 70 nm spacer. Exemplarily, let us focus on the latter.

The two ESR peaks shown in Fig. 4 are characterized by *g* factors of about 1.9992 (*R*) and 1.9994 (*L*) (with the magnetic field in growth direction) and by different intensities. The stronger peak *R* is the one with the lower *g* factor. When the magnetic field is turned toward the in-plane direction of the quantum dots, the signals broaden and cannot be resolved [Figs. 4(a) and 4(b)]. By varying the microwave power, the relative intensity of the two peaks changes. At low powers, *L* is almost not visible which makes further characterization of *R* possible [Fig. 4(b)]. By changing the orientation of the sample with respect to the external magnetic field, again an anisotropy in the linewidth [Fig. 4(c)] and of the *g* factor of *R* becomes apparent [Fig. 5(b)]. The linewidth broadens from $\Delta H_{pp}\approx 0.12$ Oe to $\Delta H_{pp}\approx 0.32$ Oe. The *g* factor of *R*

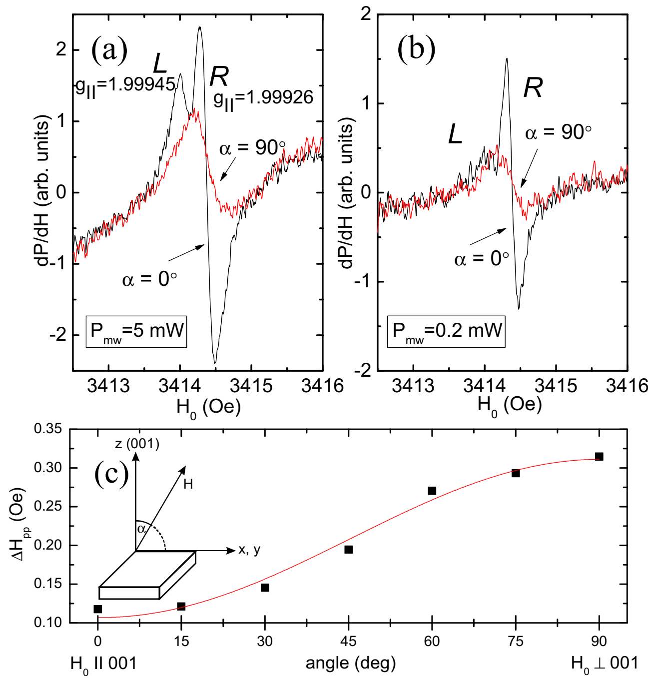

FIG. 4. (Color online) Spectra of the sample grown at 700 °C and with 70 nm spacer (a) $g_{\|}(R)=1.99926$ and $g_{\|}(L)=1.99945$ at $P_{mw}=5$ mW and (b) $P_{mw}=0.2$ mW; (c) linewidth of the peak with lower g factor (R) and schematic of sample orientation. Angle α indicates the direction of the external magnetic field from the (001) direction ($\alpha=0°$) to the perpendicular direction ($\alpha=90°$).

shows an axial symmetric anisotropy with $g_{\|}(R)=1.99926(2)$, $g_{\perp}(R)=1.99914(2)$, and $\Delta g=1.2\times10^{-4}$.

Unfortunately, a complete characterization of L is not possible for this sample since even for the highest microwave power below saturation, the contribution from R cannot be separated completely from L as the sample is turned toward the in-plane direction. Because of that, L is only characterized in an angle of $\pm20°$ around $\alpha=0°$, $H_0\|(001)$ for which the lines are still resolved yielding $g_{\|}(L)=1.99945(2)$. When assuming the same axial symmetry derived for $g(R)$, the

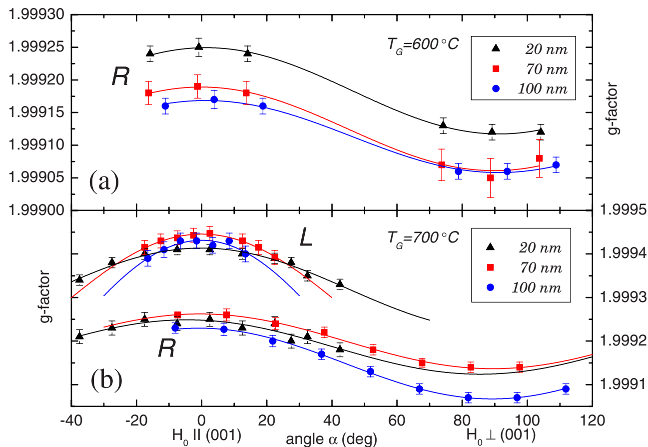

FIG. 5. (Color online) Angular dependence of the g factor determined at $P_{mw}=1$ mW; (a) samples grown at 600 °C and (b) samples grown at 700 °C. The spacer thickness is indicated.

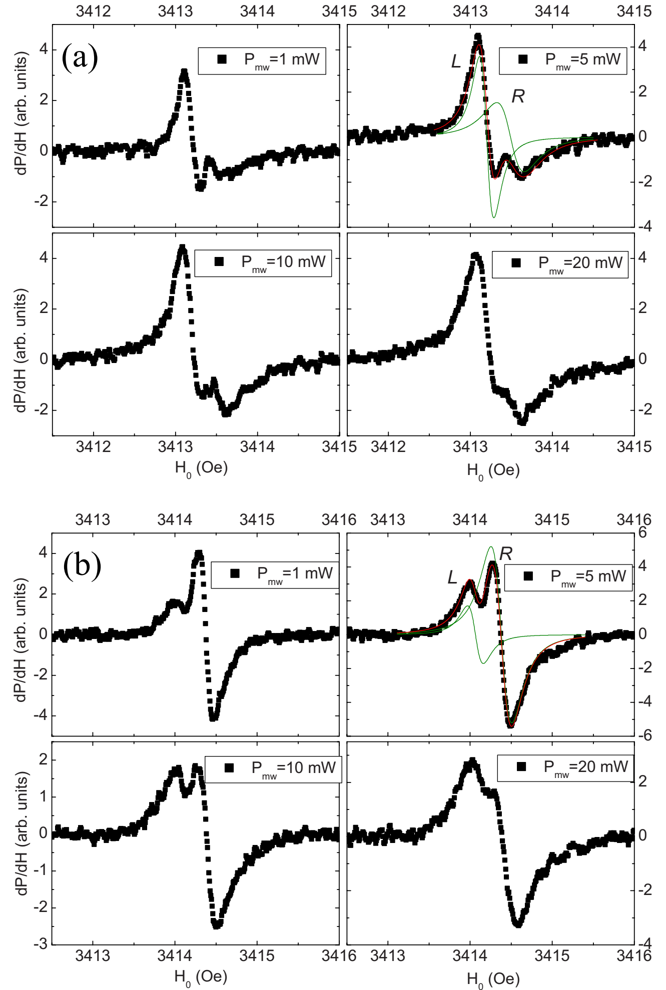

FIG. 6. (Color online) ESR spectra for selected P_{mw} from 1 to 20 mW for (a) 20 nm and (b) 70 nm Si spacer; graphs at 5 mW show data with double Lorentzian fit and the single Lorentzian lines extracted. The external magnetic field is along the growth direction (001).

value for $g_{\perp}(L)$ can be extrapolated to $g_{\perp}(L)=1.99909$ [Fig. 5(b)].

For the sample with the smallest spacing of 20 nm silicon, the spectrum looks quite different [cf. Figs. 6(a) and 6(b)]. Still two peaks are observed but with L having higher intensity. Nevertheless, the g factor corresponding to L and R for different samples is almost identical regardless the change in relative intensity. This indicates that L and R originate from individual spin states which are present in all samples.

The integrated intensity of the ESR signal below saturation is proportional to the number of resonating spins contributing to the signal. Thus, in a nonsaturated regime for both signals, their relative intensity gives information about the relative population of those two states. For 100 and 70 nm, the integrated intensity ratio is about $L/R\simeq1/5$ while for the 20 nm sample, it is about $L/R\simeq1/1$. Thus, a drastic change in the relative population of the two states takes place as the distance between the dots is decreased.

Due to this transfer of the spectral weight, both peaks can only be determined in an angle of $\pm40°$ around $g_{\|}$. The g

values for R are the same as for the 20 nm spaced dots grown at 600 °C.

Since the g-factor anisotropy of L is stronger, the two lines merge upon rotation of the field toward the sample plane and are not resolved anymore. For R alone, a broadening is observed as well.

C. T_1-relaxation time

The T_1-relaxation time characterizes the rate of the transfer of the excess energy from the spin ensemble in a magnetic field to the environment. Usually this is due to the interaction with phonons, conduction electrons, nuclear spins, etc. This time can be probed in continuous-wave ESR by applying different microwave radiation powers. At high microwave powers, the thermal equilibrium between the split spin orientations in magnetic field is disturbed. This is visible as a saturation and an eventual decrease in the ESR signal. By determining the saturation power, the relaxation time can be calculated. For the power resulting in the maximal derivative amplitude of the ESR signal, T_1 is given by[19]

$$T_1 = \frac{0.49 \times 10^{-7} \Delta H_{pp}[\mathrm{Oe}]}{g H_1^2 [\mathrm{Oe}^2]} [\mathrm{s}]. \quad (1)$$

It has to be noted that the microwave magnetic field H_1 at the sample is calculated from the known calibration of the resonator without quartz cryostat. The real H_1 might be different due to the quartz cryostat and the microwave conductivity of the sample itself. Therefore values obtained for T_1 cannot be very precise. In addition, the weak intensity makes it difficult to find the exact saturation point. Nevertheless, an order of magnitude estimate of T_1 yields a value on the order of $T_1 < 10$ μs. Typically relaxations times of L are slightly longer than those of R.

D. T_2-relaxation times

The dissipation of the irradiated microwave energy within the spin ensemble is characterized by the T_2-relaxation time, which is the time of an irreversible loss of the phase coherence of the spin ensemble. If individual spins experience different local fields, their precession dephases at a time T_2^*. This dephasing time can be much shorter than the coherence time T_2. In contrast to the T_2 process, the T_2^* process is not a true relaxation process. It is, in general, reversible and does not affect the T_1 and T_2 times.

Because of $T_2 \leq T_2^*$ in continuous-wave ESR, the linewidth is directly related to the dephasing time T_2^*. An ESR line can be broadened by different mechanisms. If the internal magnetic field itself or the g factor is inhomogeneous over the sample, microwave radiation will be absorbed at different external magnetic fields. The statistical distribution of Lorentzian lines over the field results in a Gaussian line shape of the ESR signal. Also an anisotropic dipole-dipole interaction between spins can result in a broadening of the line. However, exchange interaction between spins can narrow the line again, which results in a Lorentzian line shape. From the linewidth below saturation, the dephasing time T_2^* can be calculated as[19]

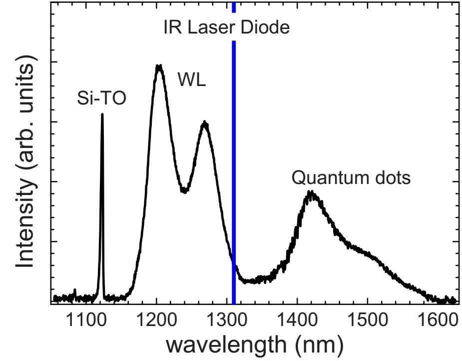

FIG. 7. (Color online) Low-temperature (about 8 K) photoluminescence of the SiGe quantum-dot multilayer grown at 700 °C with 100 nm spacing. Si peak, wetting-layer, and SiGe quantum-dot emissions are indicated as Si-TO, WL, and quantum dots, respectively. The blue line marks the laser excitation wavelength $\lambda = 1310$ nm used in ESR measurements.

$$T_2^* = \frac{1.3131 \times 10^{-7}}{g \Delta H_{pp}[\mathrm{Oe}]} [\mathrm{s}]. \quad (2)$$

Linewidths [Fig. 4(c)] correspond to T_2^* times ranging from $T_2^* \approx 0.5$ to ≈ 0.2 μs. This provides a lower limit for the T_2 spin coherence time.

E. Effect of illumination

Samples were illuminated with light at wavelengths of $\lambda_1 = 655$ nm (red) or $\lambda_2 = 1310$ nm (infrared—IR). This corresponds to energies $E_1 = 1.5$ eV and $E_2 = 0.95$ eV, respectively. With the Si band gap being at $E_g = 1.1$ eV electron-hole pairs in Si can be generated with the red laser. Ionization of the shallow donors and acceptors in Si (for instance, phosphorus and boron $E_P \simeq E_B \simeq 45$ meV) also takes place. Looking at photoluminescence measurements of the samples[20] (see Fig. 7), it is evident that the excitation wavelength of the IR laser is below the Si band gap and even partially below the wetting layer. On the other hand, the quantum-dot emission is well below the IR excitation energy.

While no ESR signal could be found in any reference sample without light, an ESR signal around $g = 1.9995$ was observed on those samples under illumination with the red laser light ($\lambda_1 = 655$ nm). This g factor is identical with the g factor of conduction-band electrons in Si. The linewidth is similar to the one reported previously for bulk silicon[21] $\Delta H \approx 1$ Oe. Since the g factors of conduction-band electrons and electrons on quantum dots are very close so that their ESR signals might overlap, the experiments focus on illumination with subband-gap light.

For the subband-gap IR laser, no additional signal in all reference structures can be seen. In contrast to that, in the quantum-dot structures, the already visible signal increases significantly (Fig. 2).

By illuminating the quantum-dot samples grown at 600 °C, the intensity of the single ESR peak increases strongly. The increase does not go along with a change in the linewidth which would indicate a faster relaxation. Thus, it

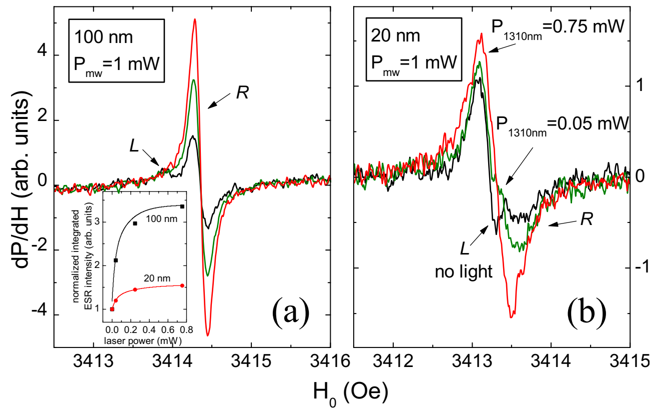

FIG. 8. (Color online) Signal intensity with illumination at different laser powers compared to the spectrum without illumination; (a) 100 nm sample at $P_{mw}=1$ mW, (b) 20 nm sample at $P_{mw}=1$ mW; inset to (a): normalized integrated ESR intensity as a function of incident laser power for both samples.

can be interpreted as a pure increase in the number of spins giving rise to the ESR signal.

More interesting is the behavior of the double-peak spectra: The two signals are amplified differently under illumination with subband-gap light. For the 100 nm sample at a microwave power of 1 mW [Fig. 8(a)], the two peaks are well separated for the spectrum without illumination and only R is increasing in intensity upon illumination. From the data, it is not clear if L is simply masked by R or if it is even decreasing in intensity. Thus, the electronic state corresponding to R gets populated under illumination, revealing a nonlinear dependence on the laser power for the integrated ESR intensity [Fig. 8(a), inset].

For the 20 nm sample, the two peaks are also nicely visible at a microwave power of 1 mW in the spectrum without illumination [Fig. 8(b)]. Upon illumination with only a small laser power, L decreases while R increases. By increasing the laser power, R increases further and L is not visible anymore. This indicates a shift in population from L (or the electronic state giving rise to L) to R at first, and, with higher light intensity, a continuous increase in the population of the R state.

We rationalize the above observations as follows. In silicon at temperatures around 4 K, most of the electrons are localized at shallow donors and the electron concentration in the conduction band is small. Upon illumination with above band-gap light, electrons are excited from the valence to the conduction band. This increase in the electron concentration makes observation of the conduction-band electrons with ESR possible even at low temperatures.[21] Besides the direct generation of carriers from the valence band, ionization of donors takes place as well. Illuminating at a wavelength of $\lambda_2=1310$ nm, with an energy well below the band gap of silicon and below the wetting-layer emission energy, the ionization of donors is the major process providing conduction-band electrons in the reference structures. The concentration in the conduction band is increasing but is much lower than for the electron-hole generation from the valence band with above band-gap light. The ionization of donor electrons alone does not provide a sufficient amount of conduction-band electrons that could be detected by cw ESR. Furthermore, if quantum dots are present, electrons may also be generated by direct absorption of photons on the quantum dots. Consequently, electrons are trapped on the quantum dots, resulting in an increase in the signal.

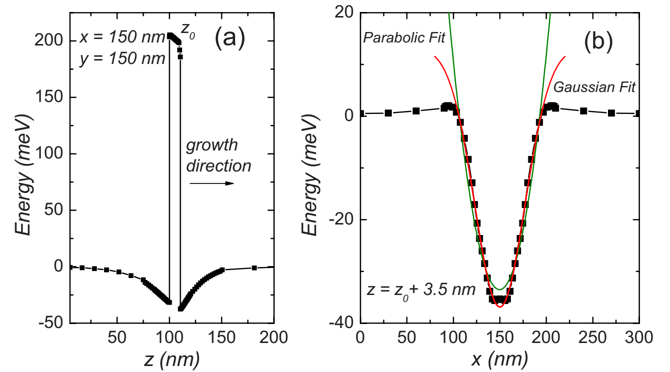

FIG. 9. (Color online) Conduction-band profiles calculated with the program NEXTNANO³ for a semiparabolic quantum dot with height $h=10$ nm, base diameter $d=80$ nm, and Ge content of 36%. $E=0$ corresponds to the unstrained conduction band in Si. (a) In z direction, it shows a sharp edge for the penetration of the wave function in the quantum dot and a smooth increase away from it. (b) In the xy plane, the confining potential can be approximated by a Gaussian form.

IV. ELECTRONIC STRUCTURE OF QUANTUM DOTS

A SiGe quantum dot induces strain in the Si matrix around it. Above the top of the dot, the Si will be under tensile strain. This translates into a hydrostatic component and a uniaxial compressive strain in growth direction. This strain shifts and splits the lowest-lying sixfold-degenerate conduction Δ band. A confining potential for electrons is formed by the Δ_2 bands which are lowered in energy. The change in the potential is small over the range of the lattice constant. Therefore an effective-mass approximation is still valid and the electrons can be described as Δ_2-band like.

Structural parameters were extracted from AFM and TEM images and their statistical analysis and were used as input data for the calculations. Structures were simulated with the program NEXTNANO³ (see Ref. 22) assuming semiparabolic SiGe quantum dots. Similar calculations with this program on SiGe nanostructures have been performed before.[23] As corroborated by TEM analysis, buried islands in the subsequent layers are similar in size and form. As a consequence, we performed calculations focusing on a single SiGe nanostructure surrounded by a Si matrix. Results for a dot with 80 nm base diameter are shown in Figs. 9 and 10. A magnetic field H of 3400 Oe is applied along the growth direction z.

Looking at the single dot structure, the potential in z direction (growth direction) shows a sharp edge at the boundary between SiGe and Si [Fig. 9(a)]. From there it increases smoothly until the conduction-band energy reaches that of the unstrained Si. At the boundary, the potential is similar to a single interface of a modulation-doped quantum well. In the perpendicular plane, the confining potential is close to a

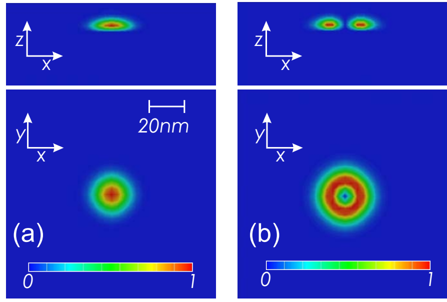

FIG. 10. (Color online) (a) s-like-state and (b) p-like-state probability wave functions for a magnetic field $H=3400$ Oe in z direction.

Gaussian or parabolic form [Fig. 9(b)]. The wave functions calculated in the effective-mass approximation for discrete states have a pancakelike form and extend over more than 20 nm in-plane but less than 10 nm in z direction. s- and p-like-state wave functions are shown in Fig. 10. When increasing the size of the quantum dots (up to 200 nm base diameter—corresponding to dots grown at 700 °C), the wave-function extension increases in the xy plane. Furthermore, the energy splitting between eigenstates on the same dot becomes smaller.

The electron s-like-wave functions is centered in the silicon on top of the dot, directly at the SiGe/Si interface z_0. With the spatial extensions of the wave functions significantly larger than the Bohr radius in Si, the dot might act as a single heterointerface. This barrier effect will be different for the p state, which has a node at the apex of the dot and extends larger in-plane. When regarding the top of the dot as a single heterointerface, the problem of a confined electron under uniaxial stress may not be described by the T_d symmetry found for donor states in bulk Si or Ge (Ref. 24) anymore.

Still, an anisotropic g factor is expected since the discrete states at the quantum dots are not spherically symmetric. The s state is expected to have a stronger anisotropy following more closely the confining potential. Note that such an effect (much stronger in magnitude) was already observed in InGaAs quantum dots.[25]

While electronic states for 70 and 100 nm spacing are only seeing one SiGe/Si barrier, the electronic states for 20 nm spacing are expected to be confined in between two barriers but the effect on the wave function is small.

V. DISCUSSION

A. Assignment of lines

In general, dots grown at 600 °C are smaller in size with an average Ge content of about 50%. For those dots, the areal coverage is higher and thus the average number of donors per dot is lower. Still it is sufficient for s states to be filled completely and p states to be partly populated. An ESR signal can only be observed from unpaired electrons. This means completely filled levels—up and down spin—are ESR silent. Therefore, the single peak observed, which shows very small anisotropy in g factor, can be attributed to electrons in a p state.

Since we are dealing with an ensemble of dots, their confining energies differ throughout an individual sample. This is especially important for the dots grown at 700 °C. Structures grown at higher temperatures have higher intermixing and therefore are larger. Calculations for a (single) large quantum dot show that the energy difference $\Delta E_{\rm sp}$ between s and p states decreases from about 2 meV to about 0.4 meV. Already the thermal energy at 4 K can therefore lead to differently populated levels. This can result in individual dots where the s state is only partly populated.

The left peak L observed in the doublets (Fig. 6) is therefore attributed to electrons in the s states. The right peak R shows a behavior which is very similar in g factor to the peak observed for the structures grown at 600 °C and can be identified as originating from the p states.

Dots spaced 100 nm apart can surely be regarded as isolated. But let us consider the situation when the dots are brought closer together. With a smaller vertical spacing between the quantum-dot layers and a height of the quantum dots of roughly about 10 nm, quantum dots are aligned vertically. This results in an accumulation of strain in between the quantum dots, leading to a deeper potential. Their size is not significantly different for aligned dots in different layers. However, the overall size distribution becomes wider. No change in the relative population of the two peaks is observed changing the spacer from 100 to 70 nm, indicating that the absolute energy of the confined state does not play a dominant role for a certain occupation.

The shift in the spectral weight, as the spacing between quantum-dot layers is decreased to 20 nm, reflects a change from favored p-state to s-state population [compare Figs. 6(a) and 6(b)]. This can be explained by the higher number of dots in this particular structure, thus a smaller donor/dot ratio, which is equivalent to a lower occupation of a single dot on average. Furthermore, because of the strain accumulation, more dots are present with confining states below the Fermi energy, which also results in a lower occupation for the single dot.

The ESR experiments with sub-Si band-gap light illumination further support the above assignment of the signals. Under illumination with light, the electron concentration is increased by ionization of donors. By illuminating over the time of the measurement, an increased equilibrium Fermi level is established. Alternatively a generation of electron-hole pairs from the quantum dots is possible as well. However, dots are not excited resonantly so that electrons are pumped (directly) in higher states and then relax back to the lowest unoccupied state.

In both possible scenarios, electrons from the conduction band are trapped in the potentials around the nanostructures populating additional dots and higher states in the individual potentials. Confined levels are filled from the lowest unoccupied state first. As more levels are filled, the s-state ESR signal decreases. At the same time, p states are getting more and more populated but not yet filled. Therefore the increase in the intensity of the R ESR signal under illumination with subband-gap light means a further population of the p states and a filling of the s state [Fig. 8(b)].

B. Relaxation and dephasing time

Due to the small size and shape variation in the ensemble of quantum dots, it is not expected that g factors are identical. This causes a broadening of the ESR line. However, the spread in g factors is obviously smaller than the difference in g factors between the two resolved lines observed ($\Delta g \simeq 2\times 10^{-4}$). Considering the above-mentioned mechanisms of the inhomogeneous broadening, the ESR signal of the ensemble of spins should show a Gaussian line. Because all lines observed are of a Lorentzian form, there has to be a mechanism present that narrows the line again. Since the quantum dots are occupied by several electrons, the isotropic exchange interaction between the spins at the same quantum dot seems to be the primary source of the line narrowing. Such interaction is within the spin ensemble and therefore can significantly enlarge the T_2^* time, whereby it does not affect the T_1 time directly. A secondary narrowing effect could be due to the interdot exchange interaction. However, we did not find a direct correlation between average interdot distance and the linewidth.

The estimated T_1 times of about 10 μs are slightly longer than what was observed in Si/SiGe quantum-well structures[9] but significant shorter than that of donor states in silicon.[26] Since the electrons on the quantum dots are spatially not as strongly confined as on the donors this value seems reasonable. The T_1 time is larger than the T_2^* times of about 0.5 μs, suggesting that the spin-lattice relaxation does not contribute substantially to the spin dephasing at low temperatures. However, as the spin coherence time T_2 could be longer than T_2^*, the spin lifetime T_1 could be a limiting factor for spin coherence on SiGe quantum dots.

VI. CONCLUSION

We used electron spin resonance to study in detail electrons confined by SiGe nanostructures. Two resonances were detected which were attributed to s- and p-like states of confined electrons on the quantum dots. By applying subbandgap illumination, the relative population between the states can be changed. g factors are close to the free-electron g factor showing only a small anisotropy with an axial symmetry. The well-separated lines for an ensemble of quantum dots show that the influence of strain, and thus confining energy on the g factor is small compared to the effect of spin-orbit coupling on the two different states. The anisotropy is stronger for the s-like state. Structural differences determine the confinement of electrons and with that the population of dots under constant doping.

The separation and characterization of the two states on quantum dots might enable selective spin control with established ESR techniques. The fact that both lines can be observed even for broad ensembles enables fairly low requirements on sample quality, which is advantageous for development of devices. However, structures have to be optimized in order to increase the signal/noise ratio.

ACKNOWLEDGMENTS

This work was supported by the Deutsche Forschungsgemeinschaft (DFG) within a nonlocal DFG research unit “Coherence and relaxation properties of electron spins” (Grant No. FG-912). We acknowledge B. Rellinghaus and T. Gemming for the use of TEM. We thank V. Fomin for many helpful discussions.

[1] *Spin Physics in Semiconductors*, Springer Series in Solid-State Sciences Vol. 157, edited by M. I. Dyakonov (Springer, New York, 2008).

[2] A. V. Khaetskii, D. Loss, and L. Glazman, Phys. Rev. Lett. **88**, 186802 (2002).

[3] G. Feher, Phys. Rev. **114**, 1219 (1959).

[4] A. Ferretti, M. Fanciulli, A. Ponti, and A. Schweiger, Phys. Rev. B **72**, 235201 (2005).

[5] L. M. Roth and B. Lax, Phys. Rev. Lett. **3**, 217 (1959).

[6] G. Feher, D. K. Wilson, and E. A. Gere, Phys. Rev. Lett. **3**, 25 (1959).

[7] D. K. Wilson and G. Feher, Phys. Rev. **124**, 1068 (1961).

[8] G. Abstreiter, H. Brugger, T. Wolf, H. Jorke, and H. J. Herzog, Phys. Rev. Lett. **54**, 2441 (1985).

[9] A. M. Tyryshkin, S. A. Lyon, W. Jantsch, and F. Schaffler, Phys. Rev. Lett. **94**, 126802 (2005).

[10] Z. Wilamowski, W. Jantsch, H. Malissa, and U. Rossler, Phys. Rev. B **66**, 195315 (2002).

[11] Ch. G. Van de Walle and M. M. Richard, Phys. Rev. B **34**, 5621 (1986).

[12] O. G. Schmidt, K. Eberl, and Y. Rau, Phys. Rev. B **62**, 16715 (2000).

[13] K. Brunner, Rep. Prog. Phys. **65**, 27 (2002).

[14] H. Malissa, W. Jantsch, G. Chen, D. Gruber, H. Lichtenberger, F. Schäffler, Z. Wilamowski, A. M. Tyryshkin, and S. Lyon, Mater. Sci. Eng., B **126**, 172 (2006).

[15] A. F. Zinovieva, A. V. Dvurechenskii, N. P. Stepina, A. S. Deryabin, A. I. Nikiforov, R. M. Rubinger, N. A. Sobolev, J. P. Leitao, and M. C. Carmo, Phys. Rev. B **77**, 115319 (2008).

[16] J. Stangl, T. Roch, G. Bauer, I. Kegel, T. H. Metzger, O. G. Schmidt, K. Eberl, O. Kienzle, and F. Ernst, Appl. Phys. Lett. **77**, 3953 (2000).

[17] S. Lebib, M. Schoisswohl, J. L. Cantin, and H. J. von Bardeleben, Thin Solid Films **294**, 242 (1997).

[18] J. L. Cantin and H. J. von Bardeleben, J. Non-Cryst. Solids **303**, 175 (2002).

[19] Charles P. Poole, Jr., *Electron Spin Resonance: A Comprehensive Treatise on Experimental Techniques*, 2nd ed. (Dover, New York, 1996).

[20] Microphotoluminescence (μPL) investigations have been performed at about 8 K, using a cold-finger helium-flow cryostat and a 532 nm frequency-doubled Nd:YVO4 laser. The laser spot diameter on the sample surface was of about 1.5 μm with a power of about 1 mW. The same μPL microscope was then used to collect the PL emission, which is dispersed by a 500 mm focal length spectrometer, equipped with a liquid-nitrogen-cooled InGaAs array detector.

[21] C. F. Young, E. H. Poindexter, G. J. Gerardi, W. L. Warren, and D. J. Keeble, Phys. Rev. B **55**, 16245 (1997).
[22] S. Birner, T. Zibold, T. Andlauer, T. Kubis, M. Sabathil, A. Trellakis, and P. Vogl, IEEE Trans. Electron Devices **54**, 2137 (2007).
[23] D. Grutzmacher, T. Fromherz, Ch. Dais, J. Stangl, E. Muller, Y. Ekinci, H. H. Solak, H. Sigg, R. T. Lechner, E. Wintersberger, S. Birner, V. Holy, and G. Bauer, Nano Lett. **7**, 3150 (2007).
[24] W. Kohn and J. M. Luttinger, Phys. Rev. **98**, 915 (1955).
[25] T. P. Mayer Alegre, F. G. G. Hernandez, A. L. C. Pereira, and G. Medeiros-Ribeiro, Phys. Rev. Lett. **97**, 236402 (2006).
[26] G. Feher and E. A. Gere, Phys. Rev. **114**, 1245 (1959).